


## Mechanochemically controlling the van der Waals gap in molybdenum disulfide nanosheets

Vishnu Nair,<sup>\*</sup> Khagesh Kumar,<sup>\*</sup> and Chandramouli Subramaniam<sup>†</sup>

*Department of Chemistry, Indian Institute of Technology Bombay, Powai, Mumbai-400076, India*

 (Received 12 May 2018; revised manuscript received 24 November 2018; published 8 January 2019)

We report a facile mechanochemical approach to achieve precisely controlled van der Waals spacing in molybdenum disulfide ( $\text{MoS}_2$ ) nanosheets. This involves mechanochemical, solid-state grinding of bulk  $\text{MoS}_2$  with solid sodium chloride ( $\text{NaCl}$ ), resulting in intercalation of  $\text{Na}^+$  ions within the  $\text{MoS}_2$  sheets. Consequently, distinct changes to the van der Waals spacing of  $\text{MoS}_2$  is observed and attributed to coordinative adsorption followed by a diffusion-assisted intercalation. In contrast to Li-ion intercalation, the native  $2H$  structure of  $\text{MoS}_2$  is stabilized and completely preserved. Thus the resulting  $2H$ - $\text{MoS}_2$  layers exhibit expanded van der Waals spacing. Spectroscopic investigations, through time-dependent Raman and X-ray photoelectron spectroscopy, confirm the kinetics of intercalation resulting in precise tunability of van der Waals spacing from 0.61 to 1.25 nm. Such a scalable approach for tunable intercalation of nanosheets presents a route for controlling defect density in  $\text{MoS}_2$ , thereby providing directions in defect engineering and heterogeneous catalysis.

DOI: [10.1103/PhysRevMaterials.3.015802](https://doi.org/10.1103/PhysRevMaterials.3.015802)

### I. INTRODUCTION

Transition-metal dichalcogenides such as two-dimensional sheets of molybdenum disulfide ( $\text{MoS}_2$ ) have attracted increasing interest due to their edge-mediated catalytic capability and the sheet-mediated ability to reversibly intercalate alkali-metal ions for energy storage [1–8]. Accordingly, the synthesis of isolated  $\text{MoS}_2$  nanosheets has been reported through both top-down exfoliation routes and bottom-up chemical vapor deposition routes [3–5]. Highly crystalline, uniform, and defect-free  $\text{MoS}_2$  nanostructures fabricated through bottom-up approaches are ideal for fundamental investigation but possess lower edge-mediated catalytic capabilities [1,9,10]. In contrast, top-down strategies often yield a wide dispersity in the number of layers, but contain a higher degree of structural defects [11,12]. The structural defect density in such layered materials could be controlled by intercalation of suitable chemical moieties in their van der Waals gap [2,7,13]. Extensive chemical, electrochemical, gas-phase, and organometallic approaches have been reported for achieving intercalation of alkali-metal ions into the layered framework of  $\text{MoS}_2$  to obtain structures with expanded van der Waals spacing [1]. However, such studies have also observed a simultaneous phase transformation from  $2H$  to  $1T$  form in  $\text{MoS}_2$  nanostructures [1]. The structural transformation leads to a change from semiconductor ( $2H$ ) to metallic ( $1T$ ) form and often results in inability to investigate the catalytic properties of native  $2H$ - $\text{MoS}_2$ .

In comparison to sophisticated and expensive chemical and electrochemical techniques, easier and cheaper mechanical methods have been explored to a very less extent [1]. Moreover, it is often observed that mechanical shearing forces lead to exfoliation rather than intercalation, which simulta-

neously induces structural defects [11,12]. Thus, in order to have less exfoliation and more intercalation-induced defects, low-energy techniques like mortar-pestle grinding hold potential against ball milling and probe sonication [14]. Ambient energy techniques like mortar-pestle grinding would have sufficient energy to overcome weak van der Waals forces for diffusive intercalation and defect generation but not enough to completely shear multiple layers of the material away. This is often supported by the use of an abrasive during grinding [15].

Here, we report a one-pot scalable mechanochemical route that provides  $\text{Na}^+$  intercalated  $2H$ - $\text{MoS}_2$  with tunable van der Waals spacing and defect density. Such structures are created by surface adsorption of  $\text{Na}^+$  ions followed by their diffusion into the voids of (002) spacing in  $\text{MoS}_2$  nanosheets. This mechanism and its kinetics are studied by time-dependent Raman,  $^{23}\text{Na}$  NMR, and X-ray photoelectron spectroscopy (XPS) measurements.

### II. EXPERIMENTAL METHODS

#### A. Synthesis of intercalated $\text{MoS}_2$

The synthesis is carried out as illustrated in the schematic in Fig. 1(a). Bulk  $\text{MoS}_2$  and  $\text{NaCl}$  were taken in varying mass ratio (1:3, 1:5, 1:7, 1:9) in a mortar and ground with a pestle for 30 min to obtain a uniformly ground mixture. This mixture is then transferred to chloroform and bath sonicated for 5 min for further homogenization. This is followed by phase transfer of sodium intercalated  $\text{MoS}_2$  sheets into aqueous phase. This transfer occurs as the sodium intercalated sheets are now positively charged and require negatively charged chloride ions to solvate them to give a neutral ionic-like species. The aqueous layer after separation from the organic phase is allowed to stand up to 36 h in a constant-temperature bath maintained at 298 K. This is to allow further diffusion of sodium ions into the van der Waals gap such that we get uniform intercalation. The intercalated nanostructure finally

<sup>\*</sup>V.N. and K.K. contributed equally to this work.

<sup>†</sup>Corresponding author: [csbbu@chem.iitb.ac.in](mailto:csbbu@chem.iitb.ac.in)

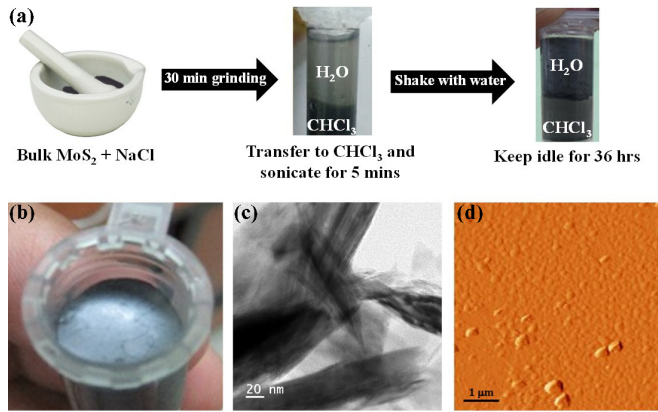


FIG. 1. (a) Schematic depicting the synthesis of the intercalated  $\text{MoS}_2$  structure. (b) Films of intercalated  $\text{MoS}_2$  assembled at air-water interface. (c) TEM micrograph illustrating nanoscale morphology of intercalated  $\text{MoS}_2$ . (d) AFM of assembled films revealing that the films are discontinuous and composed of smaller fragments.

assembles at the air-water interface as a layer [Fig. 1(b)]. These layers can be scooped out using a copper loop (see Supplemental Material, Ref. [16]) and transferred to any substrate for further analysis. These samples are designated as M13, M15, M17, and M19 according to the  $\text{MoS}_2$ :NaCl weight ratio used for their preparation. For performing time-dependent studies samples which self-assembled at the air-water interface at 0, 12, 24 and 36 h after the phase transfer step are scooped out and placed on a clean glass slide, silicon wafer, or a formvar transmission electron microscopy (TEM) grid.

### B. Characterization techniques

TEM and selected area electron diffraction (SAED) was carried out on a JEOL-JEM 2010F instrument with a field-emission gun at an accelerating voltage of 200 kV. Atomic force microscopy (AFM) was carried out on Asylum/Oxford Instruments MFP3D Origin in contact mode, XPS was done on Kratos Analytical AXIS Supra with Al  $K\alpha$  X-ray source. Raman spectroscopy was performed in a backscattering geometry using a WiTec micro-Raman spectrometer and a Nd-yttrium aluminum garnet laser of 532 nm. Microphotoluminescence (PL) measurements were done using a 490-nm-diode laser and a spot size of 350 nm, and power up to 2 mW. Sodium NMR measurements were done on VARIAN, Mercury Plus 300 MHz NMR. Raman measurements were done on a glass substrate and XPS on Si wafer.

## III. RESULTS AND DISCUSSION

### A. Microscopic characterization

Self-assembled films of the  $\text{Na}^+$  intercalated  $\text{MoS}_2$  formed at the air-water interface after 36 h were transferred using a clean copper wire loop onto a silicon wafer and copper grid to perform AFM and TEM, respectively. The AFM profile of the sample on a micrometer scale reveals that the nanostructured film is made up of distinct fragments [Fig. 1(d)]. The AFM height profile exhibits an average thickness of

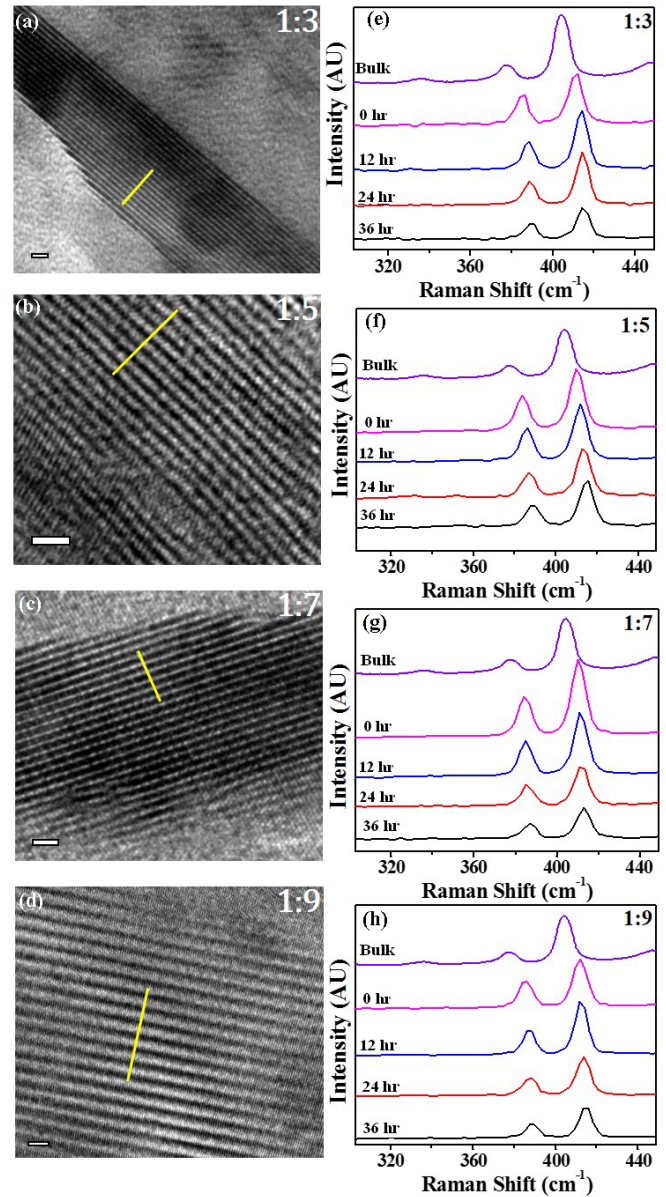


FIG. 2. TEM micrographs showing intercalated structure of (a) M13, (b) M15, (c) M17, and (d) M19 isolated at 36 h (all scale bars are 2 nm). Time-dependent Raman measurements showing intercalation in structures synthesized of (e) M13, (f) M15, (g) M17, and (h) M19.

43.9 nm, indicating the presence of  $\sim 70$  layers of  $\text{MoS}_2$  [16]. High-resolution TEM (HR-TEM) images of these fragments, prepared with different mass loading of NaCl, exhibit layered  $\text{MoS}_2$  with varying van der Waals spacing. Significantly, a monotonic increase in the van der Waals spacing is observed with increasing mass ratio of NaCl [Fig. 3(a)]. Thus, we can observe that the van der Waals or (002) spacing of layered  $\text{MoS}_2$  can be precisely controlled and tuned from 0.61 nm in bulk to 1.25 nm in M19. Upon increasing the weight ratio of NaCl further, a systematic increase in the (002) spacing is noticed [Figs. 2(a)–2(d), 3(a)]. Thus, varying the  $\text{MoS}_2$ : NaCl ratio from 1:3 to 1:5, further to 1:7 and finally 1:9 resulted in an increase of the van der Waals spacing from 0.66 to 0.71 nm,

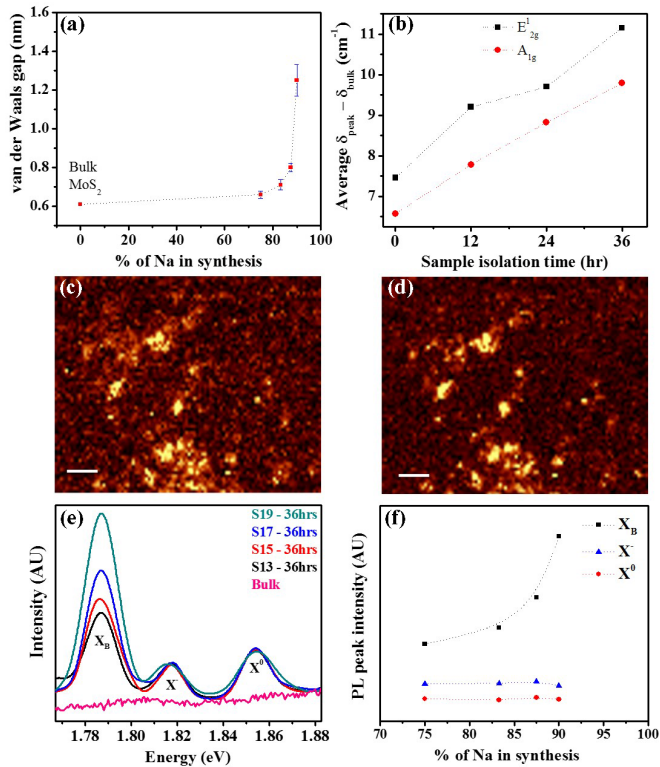


FIG. 3. (a) Variation of van der Waals gap with percentage of NaCl used for synthesis in comparison with bulk MoS<sub>2</sub> value from literature (error bars calculated based on spacing profiles in Ref. [16]). (b) Time-dependent blue shift in  $E^1_{2g}$  and  $A_{1g}$  with respect to bulk MoS<sub>2</sub>, averaged with respect to different ratio of NaCl used in synthesis. Representative Raman map of (c)  $E^1_{2g}$  peak and (d)  $A_{1g}$  of an S19 sample isolated at 36 h (scale bars are 5  $\mu\text{m}$ ). (e) Micro-PL spectra of intercalated samples isolated at 36 h, for synthesis carried out with varying concentration of NaCl in comparison with bulk MoS<sub>2</sub>. (f) Variation of excitonic luminescence peak intensity in (e) with percentage of NaCl used in synthesis.

further to 0.80 nm, and ultimately to 1.25 nm, respectively [Figs. 2(a)–2(d), 3(a)]. This trend is further supported by the HR-TEM profiles on each weight ratio of MoS<sub>2</sub>:NaCl [16]. SAED performed on all these samples gave us a pattern corresponding to 001 zone indicating high crystallinity and 2H-phase of MoS<sub>2</sub> [3,4,16]. Thus from the AFM, TEM, and SAED we can conclude that the assembled film is made up of fragments; they have an expanded and controllable van der Waals spacing with possible stabilization in the 2H phase.

### B. Structural investigations

Raman spectra were obtained on intercalated samples prepared by varying the MoS<sub>2</sub>:NaCl ratio. The characteristic  $E^1_{2g}$  and  $A_{1g}$  peaks associated with 2H-MoS<sub>2</sub> are observed in all the samples. Bulk MoS<sub>2</sub> scatters at 377 and 404  $\text{cm}^{-1}$ , which correspond to the  $E^1_{2g}$  and  $A_{1g}$  peaks, respectively [Figs. 2(e)–2(h)]. In contrast, all the MoS<sub>2</sub> layers obtained immediately after self-assembly at the air-water interface (0 h) exhibited a strong blue shift by 7  $\text{cm}^{-1}$ , providing concrete evidence for the adsorption or intercalation of Na<sup>+</sup> restricting the in-plane and out-of-plane vibrations [Figs. 2(e)–2(h),

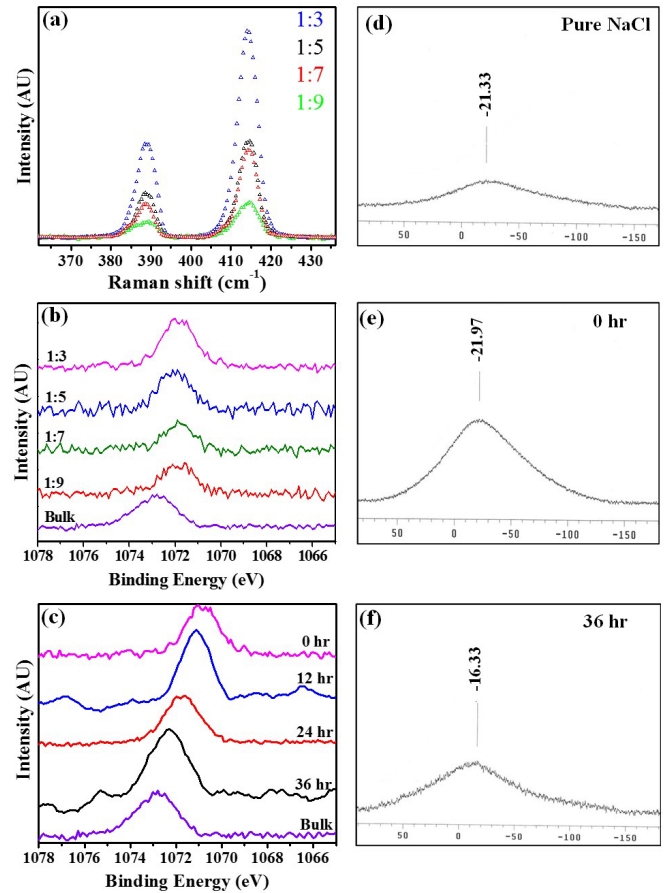


FIG. 4. (a) NaCl ratio-dependent Raman collected for samples isolated at 36 h. (b) NaCl ratio-dependent sodium XPS collected for samples isolated at 36 h. (c) Time-dependent XPS collected for M17 samples; <sup>23</sup>Na NMR ( $X$  axis - chemical shift in ppm) collected for (d) bulk NaCl, (e) M17 sample at 0 h, and (f) M17 sample at 36 h.

3(b)]. Subsequently, the spectra recorded with samples collected at 36 h of self-assembly at the air-water interface reveal further blue shift in the  $E^1_{2g}$  and  $A_{1g}$  peak to 388 and 414  $\text{cm}^{-1}$ , respectively [Figs. 2(e)–2(h), 3(b)]. Importantly, vibrational characteristics of these samples do not exhibit any dependence on ratio of MoS<sub>2</sub> and NaCl [Fig. 4(a)]. However, a gradual decrease in the intensity of both peaks is observed with increasing MoS<sub>2</sub>:NaCl ratio [Fig. 4(a)]. This indicates that both in-plane ( $E^1_{2g}$ ) and out-of-plane ( $A_{1g}$ ) vibrations are getting increasingly restricted as more NaCl is being adsorbed or intercalated and more interstitial sites are being occupied [3,9,17]. Marginal fluctuation in the energy difference between  $E^1_{2g}$  and  $A_{1g}$  peak in bulk versus the intercalated species formed under different conditions indicates that exfoliation is minimal in our synthetic process [3,9,11,16,17]. These observations are further supported by AFM profiles of the MoS<sub>2</sub> fragments composed of multiple layers with thickness varying on the order of tens of nanometers [16].

To further understand the role of NaCl ratio, XPS measurements were carried out for samples prepared with different MoS<sub>2</sub>:NaCl ratio, isolated after 36 h of self-assembly at the air-water interface. The Na<sup>+</sup> binding energy was observed at 1072 eV compared to bulk NaCl with a binding energy

of 1073 eV [Figs. 4(b) and 4(c)]. Sodium ion in bulk NaCl has greater crystal-field stabilization energy and thereby exhibits a higher binding energy compared to the sodium ion intercalated within the MoS<sub>2</sub> layers [18–20]. The order of difference of 1 eV in binding energy between bulk and intercalated form agrees with computational predictions, which reinforce the fact that this is due to intercalation [4,21,22]. However, the absence of any change in binding energy with MoS<sub>2</sub>:NaCl ratio is in excellent agreement with Raman observations and confirms that the amount of NaCl employed in the mechanochemical process does not influence the energetics of intercalation. The gradual decrease in both Raman peaks ( $E_{12g}^1$  and  $A_{1g}^1$ ) with MoS<sub>2</sub>:NaCl ratio along with invariant binding energy confirms that the ratio controls the extent of intercalation and does not influence the nature of adsorption and intercalation sites [Fig. 4(a)]. The ratio of NaCl thus plays a probabilistic role in the intercalation and not a mechanistic role [21,22]. The probabilistic role comes into the picture due to the availability of both tetrahedral and octahedral interstitial sites, with very close coordination energies, available in the van der Waals gap of MoS<sub>2</sub> [21,22]. Moreover, the presence of both  $E_{12g}^1$  and  $A_{1g}^1$  peaks in the final material irrespective of the ratio of NaCl confirms that we have retention of the 2H phase of MoS<sub>2</sub> [4]. This is in contrast with conventional intercalation techniques which would give the 1T phase upon intercalation [4–8,13,21,23].

To further investigate the properties of defects introduced by this mechanochemical technique, micro-PL measurements were carried out on samples synthesized with various ratios of NaCl, isolated at 36 h. The PL spectra clearly reveal three excitonic peaks corresponding to sulfur defect bound excitons ( $X_B$ ), charged excitons ( $X^-$ ), and free exciton ( $X^o$ ). An increasing intensity for sulfur defect bound excitons ( $X_B$ ) at 1.79 eV was observed with the ratio of NaCl in synthesis [Figs. 3(e) and 3(f)] [24–26]. This suggests that the grinding process is very efficient in introducing and modulating the defect density produced by this mechanochemical method. The charged exciton ( $X^-$ ) (1.82 eV) and free exciton ( $X^o$ ) (1.82 eV) at the direct band gap are also clearly visible in comparison with bulk [Figs. 3(e) and 3(f)] [26–28], revealing the quasi-freestanding monolayer nature of these intercalated films [27]. The appearance of a clear, well-resolved charged  $X^-$  exciton, a trion-like species, is also indicative of localized charge accumulation in the system [24–26]. Such localized charge accumulation and polarization are favorable on catalytic interfaces for carrying out redox reactions [28]. The bulk sample however lacks reduced dimensionality for any electronic wave-function localization to exhibit exciton peaks [24–26].

### C. Time-dependent mechanistic studies

Having ruled out the mechanistic role of NaCl ratio in the synthesis, herein we perform time-dependent measurements to understand the kinetics of intercalation process. We observe a monotonic blue shift in the  $E_{12g}^1$  and  $A_{1g}^1$  peaks with increasing time of the assembly at the air-water interface allowing more diffusion [Figs. 2(e)–2(h)]. This is consistent for all samples irrespective of the MoS<sub>2</sub>:NaCl ratio. However, the magnitude of the blue shift decreases and saturates with time

in all the samples investigated. Such a blue shift originates from constrained in-plane and out-of-plane vibrations due to the adsorption of sodium ions in the interstitial sites [3,9,29]. Such a gradual time-dependent shift arises from diffusion-assisted intercalation of the sodium ions into the van der Waals gap of the MoS<sub>2</sub> [22]. Importantly, the prominent existence of both  $E_{12g}^1$  and  $A_{1g}^1$  peaks at all times and ratio of NaCl indicates a stable 2H phase of MoS<sub>2</sub> with intercalation and reinforces the absence of a 2H to 1T phase transformation [3].

The entire time-dependent intercalation process is also followed through XPS measurements. Consistently, we observe that the sample obtained immediately after the assembly (0 h) exhibits the lowest binding energy of 1070.5 eV compared to 1073 eV for bulk NaCl [Fig. 4(c)]. This shift of ~2.5 eV in binding energy originates from the large number of adsorbed or intercalated sodium ions [4,6,18–20]. However, the time-dependent blue shift of the binding energy from 1070.5 to 1072 eV in 36 h [Fig. 4(c)] implies that the mechanical grinding drives sodium ions to occupy energetically unfavorable surface coordination or edge sites which are coordinatively unsaturated sites in the van der Waals spacing at 0 h. Further, these sodium ions gradually diffuse to occupy more favorable tetrahedral or octahedral void coordination sites by 36 h, an idea well supported by computational studies in literature [4,18–22]. This mechanism is further confirmed by <sup>23</sup>Na NMR measurements done on similar samples collected at 0 and 36 h [Figs. 4(d)–4(f)]. The <sup>23</sup>Na NMR for bulk NaCl gives a broad and flat peak around –21.33 ppm. This broad peak which tails until –150 ppm is indicative of hydrated sodium ions in crystalline NaCl [30–33].

The flat nature of this peak is indicative of low-mobility sodium which is the case of ions held strongly in their crystal lattice [30–33]. However, on mechanical grinding we can see that this flat peak becomes sharper without any shift, pointing to more mobile sodium ions in accordance with existing literature, and therefore represent sodium ions adsorbed at the edge or surface sites [30–33]. This observation along with the Raman and XPS confirm that the mechanical grinding step gets the sodium ions adsorbed on the surface and edge sites [30]. These surface and edge sites are coordinatively unsaturated and thus unfavorable for the sodium ions, as is evident from their low binding energy in XPS [9,10].

Furthermore, the <sup>23</sup>Na NMR measured for a 36-h sample shows that the peak shifts to –21.33 from –16.33 ppm and shows a shoulder peak or tail around 40–60 ppm. The positive shift of the peak is indicative of hyperfine coupling with local magnetic moments (possible in this system from a species like molybdenum), which can arise only when sodium ions intercalate into the van der Waals spacing from edges and surfaces to interact with molybdenum atoms [30]. Moreover, the peak at 36 h flattens, indicating decreasing mobility of ions which can arise only when the ions are in a favorable coordination environment with stronger interactions, in agreement with XPS studies where binding energy increases from 0 to 36 h [30–33]. Furthermore, the shoulder or tail appearing around 40–60 ppm is indicative of desolvated sodium ion and such species can exist only when the ions move into the (002) framework and get coordinated in a favorable site, and thus lose any previously coordinated water [30–33]. This observation thus confirms the diffusion of sodium ions from

the edge and surface adsorption sites into the van der Waals gap, ultimately modifying it [30]. Further, an absence of a time-dependent shift in the binding energy of molybdenum, across samples prepared with different ratio, indicate the absence of an electron transfer between sodium and molybdenum atoms [16]. This further supports the absence of a 2H-1T phase transition and portrays the intercalation process as a physical process rather than a redox process.

#### IV. CONCLUSIONS

In summary, the time-dependent Raman, XPS, and sodium NMR measurements confirm that mechanochemical grinding drives the adsorption of sodium ions onto the edge and surface sites of MoS<sub>2</sub> layers. The adsorption follows a kinetically driven probabilistic diffusion that subsequently leads to a thermodynamic control during the assembly of the MoS<sub>2</sub> layers at the air-water interface. Thus, the adsorbed ions in an aqueous environment slowly diffuse into the van der Waals gap to possibly occupy more stable coordination sites, leading to an intercalated species with expanded van der Waals gap. Controlling the ratio of NaCl to MoS<sub>2</sub> controls the fraction of

the sodium ions that can successfully participate in this process on an ensemble, thereby providing control and tunability over the van der Waals gap and defect density. Such MoS<sub>2</sub> nanostructures with tunable defect density hold promise as catalysts for petroleum direct desulfurization, charge-transfer reactions, and for developing energy storage devices.

#### ACKNOWLEDGMENTS

V.N. acknowledges an undergraduate research fellowship from Kishore Vaigyanik Protsahan Yohana (KVPY), Department of Science and Technology, Government of India (Fellowship No. SB1111264). K.K. acknowledges an INSPIRE undergraduate research fellowship, Department of Science and Technology, Government of India. C.S. acknowledges funding from DST-Nanomission program (SR/NM/TP-56/2016). The authors acknowledge sophisticated analytical instruments facility (SAIF), Central surface analytical facility, Bio-AFM facility at IIT Bombay for instrumentation. The authors would like to thank Prof. Dinesh Kabra and his Ph.D. student Nakul Jain, Department of Physics, IIT Bombay for their assistance with micro-PL measurements.

- 
- [1] J. Wan, S. D. Lacey, J. Dai, W. Bao, M. S. Fuhrer, and L. Hu, Tuning two-dimensional nanomaterials by intercalation: Materials, properties and applications, *Chem. Soc. Rev.* **45**, 6742 (2016).
- [2] J. B. Cook, H. Kim, Y. Yan, J. S. Ko, S. Robbenolt, B. Dunn, and S. H. Tolbert, Mesoporous MoS<sub>2</sub> as a transition metal dichalcogenide exhibiting pseudocapacitive Li and Na-ion charge storage, *Adv. Energy Mater.* **6**, 1501937 (2016).
- [3] X. Wang, X. Shen, R. Yu, and L. Chen, Atomic-scale clarification of structural transition of MoS<sub>2</sub> upon sodium intercalation, *ACS Nano* **8**, 11394 (2014).
- [4] S. Wang, J. Tu, Y. Yuan, R. Ma, and S. Jiao, Sodium modified molybdenum sulfide via molten salt electrolysis as an anode material for high performance sodium-ion batteries, *Phys. Chem. Chem. Phys.* **18**, 3204 (2016).
- [5] V. Nair, A. Kumar, and C. Subramaniam, Exceptional photoconductivity of poly (3-hexylthiophene) fibers through in situ encapsulation of molybdenum disulfide quantum dots, *Nanoscale* **10**, 10395 (2018).
- [6] Y. Li, Y. Liang, F. C. R. Hernandez, H. D. Yoo, Q. An, and Y. Yao, Enhancing sodium-ion battery performance with interlayer-expanded MoS<sub>2</sub>-PEO nanocomposites, *Nano Energy* **15**, 453 (2015).
- [7] S. Zhang, X. Yu, H. Yu, Y. Chen, P. Gao, C. Li, and C. Zhu, Growth of ultrathin MoS<sub>2</sub> nanosheets with expanded spacing of (002) plane on carbon nanotubes for high-performance sodium-ion battery anodes, *ACS Appl. Mater. Interfaces* **6**, 21880 (2014).
- [8] M. Acerce, D. Voiry, and M. Chhowalla, Metallic 1T phase MoS<sub>2</sub> nanosheets as supercapacitor electrode materials, *Nat. Nanotechnol.* **10**, 313 (2015).
- [9] J. Kinsgaard, Z. Chen, B. N. Reinecke, and T. F. Jaramillo, Engineering the surface structure of MoS<sub>2</sub> to preferentially expose active edge sites for electrocatalysis, *Nat. Mater.* **11**, 963 (2012).
- [10] D. Deng, K. S. Novoselov, Q. Fu, N. Zheng, Z. Tian, and X. Bao, Catalysis with two-dimensional materials and their heterostructures, *Nat. Nanotechnol.* **11**, 218 (2016).
- [11] H. Li, J. Wu, Z. Yin, and H. Zhang, Preparation and applications of mechanically exfoliated single-layer and multilayer MoS<sub>2</sub> and WSe<sub>2</sub> nanosheets, *Acc. Chem. Res.* **47**, 1067 (2014).
- [12] J. N. Coleman, M. Lotya, A. O'Neill, S. D. Bergin, P. J. King, U. Khan, K. Young, A. Gaucher, S. De, R. J. Smith, I. V. Shvets, S. K. Arora, G. Stanton, H. Kim, K. Lee, G. T. Kim, G. S. Duesberg, T. Hallam, J. J. Boland, J. J. Wang, J. F. Donegan, J. C. Grunlan, G. Moriarty, A. Shmeliov, R. J. Nicholls, J. M. Perkins, E. M. Grieveson, K. Theuwissen, D. W. McComb, P. D. Nellist, and V. Nicolosi, Two-dimensional nanosheets produced by liquid exfoliation of layered materials, *Science* **331**, 568 (2011).
- [13] H. Liu, D. Su, R. Zhou, B. Sun, G. Wang, and S. Z. Qiao, Highly ordered mesoporous MoS<sub>2</sub> with expanded spacing of the (002) crystal plane for ultrafast lithium ion storage, *Adv. Energy Mater.* **2**, 970 (2012).
- [14] M. A. Kabbani, C. S. Tiwary, P. A. S. Autreto, G. Brunetto, A. Som, K. R. Krishnadas, S. Ozden, K. P. Hackenberg, Y. Gong, D. S. Galvao, R. Vajtai, A. T. Kabbani, T. Pradeep, and P. M. Ajayan, Ambient solid-state mechano-chemical reactions between functionalized carbon nanotubes, *Nat. Commun.* **6**, 7291 (2015).
- [15] J. Zilinskas, J. Junevicius, K. Cesaitis, and G. Juneviciute, The effect of cleaning substances on the surface of denture base material, *Med. Sci. Monit.* **19**, 1142 (2013).
- [16] See Supplemental Material at <http://link.aps.org/supplemental/10.1103/PhysRevMaterials.3.015802> for Figs. S1–S5, which support claims mentioned in the main paper.
- [17] J. H. Lee, W. S. Jang, S. W. Han, and H. K. Baik, Efficient hydrogen evolution by mechanically strained MoS<sub>2</sub> nanosheets, *Langmuir* **30**, 9866 (2014).
- [18] R. Precht, S. Stolz, E. Mankel, T. Mayer, W. Jaegermann, and R. Hausbrand, Investigation of sodium insertion into

- tetracyanoquinodimethane (TCNQ): Results for a TCNQ thin film obtained by a surface science approach, *Phys. Chem. Chem. Phys.* **18**, 3056 (2016).
- [19] D. Sun, G. Jin, H. Wang, P. Liu, Y. Ren, Y. Jiang, Y. Tang, and X. Huang, Aqueous rechargeable lithium batteries using  $\text{NaV}_6\text{O}_{15}$  nanoflakes as high performance anodes, *J. Mater. Chem. A* **2**, 12999 (2014).
- [20] R. Precht, R. Hausbrand, and W. Jaegermann, Electronic structure and electrode properties of tetracyanoquinodimethane (TCNQ): A surface science investigation of lithium intercalation into TCNQ, *Phys. Chem. Chem. Phys.* **17**, 6588 (2015).
- [21] J. Shuai, H. D. Yoo, Y. Liang, Y. Li, Y. Yao, and L. C. Grabow, Density functional theory study of Li, Na, and Mg intercalation and diffusion in  $\text{MoS}_2$  with controlled interlayer spacing, *Mater. Res. Express* **3**, 064001 (2016).
- [22] H. He, P. Lu, L. Wu, C. Zhang, Y. Song, P. Gun, and S. Wang, Structural properties and phase transition of Na adsorption on monolayer  $\text{MoS}_2$ , *Nanoscale Res. Lett.* **11**, 330 (2016).
- [23] Y. Shi, Y. Wan, R. Liu, B. Tu, and D. Zhao, Synthesis of highly ordered mesoporous crystalline  $\text{WS}_2$  and  $\text{MoS}_2$  via a high-temperature reductive sulfuration route, *J. Am. Chem. Soc.* **129**, 9522 (2007).
- [24] S. Tongay, J. Suh, C. Ataca, W. Fan, A. Luce, J. S. Kang, J. Liu, C. Ko, R. Raghunathan, J. Zhou, F. Ogletree, J. Li, J. C. Grossman, and J. Wu, Defect activated photoluminescence in two-dimensional semiconductors: Interplay between bound, charged and free excitons, *Sci. Rep.* **3**, 2657 (2013).
- [25] X. Zhang, Q. Liao, S. Liu, Z. Kang, Z. Zhang, J. Du, F. Li, S. Zhang, J. Xiao, B. Liu, Y. Ou, X. Liu, L. Gu, and Y. Zhang, Poly(4-styrenesulfonate)-induced sulfur vacancy self-healing strategy for monolayer  $\text{MoS}_2$  homojunction photodiode, *Nat. Commun.* **8**, 15881 (2017).
- [26] S. S. Singha, D. Nandi, and A. Singha, Tuning the photoluminescence and ultrasensitive trace detection properties of few-layer  $\text{MoS}_2$  by decoration with gold nanoparticles, *RSC Adv.* **5**, 24188 (2015).
- [27] T. Eknapakul, P. D. C. King, M. Asakawa, P. Buaphet, R.-H. He, S.-K. Mo, H. Takagi, K. M. Shen, F. Baumberger, T. Sasagawa, S. Jungthawan, and W. Meevasana, Electronic structure of a quasi-freestanding  $\text{MoS}_2$  monolayer, *Nano Lett.* **14**, 1312 (2014).
- [28] V. Nair, B. Ananthoju, J. Mohapatra, and M. Aslam, Photon induced non-linear quantized double layer charging in quaternary semiconducting quantum dots, *J. Colloids Interface Sci.* **514**, 452 (2018).
- [29] J. Zou, C. Sole, N. E. Drewett, M. Velicky, and L. J. Hardwick, *In situ* study of Li intercalation into highly crystalline graphitic flakes of varying thicknesses, *J. Phys. Chem. Lett.* **7**, 4291 (2016).
- [30] S. Kajiyama, L. Szabova, K. Sodeyama, H. Iinuma, R. Morita, K. Gotoh, Y. Tateyama, M. Okobo, and A. Yamada, Sodium-ion intercalation mechanism in MXene nanosheets, *ACS Nano* **10**, 3334 (2016).
- [31] M. H. Whangbo, J. Rouxel, and L. Trichet, Effects of sodium intercalation in  $\text{TiS}_2$  on the electronic structure of a  $\text{TiS}_2$  slab, *Inorg. Chem.* **24**, 1824 (1985).
- [32] Z. Liu, Y. Y. Hu, M. T. Dunstan, H. Huo, X. Hao, H. Zou, G. Zhong, Y. Yang, and C. P. Grey, Local structure and dynamics in the Na ion battery positive electrode material  $\text{Na}_3\text{V}_2(\text{PO}_4)_2\text{F}_3$ , *Chem. Mater.* **26**, 2513 (2014).
- [33] Z. Jian, C. Yuan, W. Han, X. Lu, L. Gu, X. Xi, Y. S. Hu, H. Li, W. Chen, D. Chen, Y. Ikuhara, and L. Chen, Atomic structure and kinetics of NASICON  $\text{Na}_x\text{V}_2(\text{PO}_4)_3$  cathode for sodium-ion batteries, *Adv. Funct. Mater.* **24**, 4265 (2014).